J|A|C|S

A R T I C L E S

New Synthesis and Insight into the Structure of Blue Ultramarine Pigments

D. Arieli,[†] D. E. W. Vaughan,[‡] and D. Goldfarb*,[†]

Contribution from the Department of Chemical Physics, Weizmann Institute of Science, Rehovot, Israel, 76100, and Materials Research Laboratory, Pennsylvania State University, University Park, Pennsylvania 16802

Received December 31, 2003; E-mail: daniella.goldfarb@weizmann.ac.il

Abstract: A new and easy method for preparing blue sodalite pigments which involves high-temperature calcination of sodalite samples synthesized with aluminum sulfate and an organic template, is presented. Calcination generated the S_3^- and S_2^- radicals, and the effects of the Al/Si ratio and the calcination temperature on the nature and amounts of the radicals were examined. The radicals were characterized in detail by continuous wave and pulsed EPR at X- and W-band frequencies ($\sim$9 and 95 GHz, respectively) complemented by UV$-$vis measurements. The high-field electron-paramagnetic resonance (EPR) measurements allowed us to clearly resolve the g anisotropy of S_3^- and W-band electron nuclear double resonance (ENDOR) measurements detected strong coupling with extra-framework ^{23}Na cations and weak coupling with framework ^{27}Al. On the basis of the spectroscopic results and density functional theory (DFT) calculations of the g-tensors of S_3^- and S_2^- radicals, the EPR signals were attributed to three different S_3^- radicals, all with the open structure C_{2v}, that are located within the sodalite β cages. While two of these radicals are well isolated, the third one is associated with an exchange-narrowed signal originating from S_3^- radicals in nearby sodalite cages.

Introduction

The aluminosilicate sodalite minerals form a compositionally diverse group of minerals of interest in chemistry, geology, and material science.[1,2] The sodalite structure (see Figure 1)[3] is comprised of stacked cubooctahedral cages, often called β cages, having a free diameter of about 6 Å, connected to eight adjoining cages through 6-ring windows having a diameter of about 3 Å. Krypton (diameter 3.8 Å) readily fills the cages of this structure at elevated temperatures and pressures,[4] clearly showing that the structure is very flexible and the above dimensions are nominal, dependent on specific stoichiometry and temperatures. The blue sodalite, best known as *Lapis lazuli,* has been a favorite of jewelers since ancient Egyptian times.[1,5] Its color arises predominantly from substitution of S_3^- for the chloride ions in the sodalite β cages and it is resistant to air and high-temperature decomposition. Smaller concentrations of the yellow chromophore, S_2^-, are known to be present in these blue pigments as well;[6-8] hence, a variety of blue and green minerals can be found.

The synthesis of blue ultramarine pigments has been a subject of study since 1828 when Guimet made the first synthesis and thereby won a prize offered by the French Société d'Encouragment pour l'Industrie National.[5] Large-scale syntheses were based on heating a fine grade specially treated china clay mixed with sulfur and anhydrous sodium sulfate or carbonate. Carbon or pitch was further used to reduce the sodium salts to give the intercalated polysulfides Na_2S_x needed to produce the eventual vivid blue color. In other examples[6] the reaction mixtures were sodium aluminate, silica, anhydrous sodium acetate, and sulfur or zeolite, sulfur, anhydrous sodium acetate, and some soap binding agent. In each case the initial stage yielded the sodalite structure and the secondary calcination stage gave the improved blue color.[6] The royal blue color seems to be the result of three essential components: the alkali metal, the high sulfur content, and the sodalite type framework. Lindner and Reinen[1] claimed that the sulfur radicals have to be generated simultaneously with the formation of the zeolitic cages in the synthesis procedure, because the cages are not permeable for the color centers. Yet, Gobeltz et al.[7] have investigated the encapsulation of the chromophores into the sodalite structure during the synthesis and showed that at high temperature the colored sulfur species can diffuse into the sodalite structure even after it has been formed. The location of the radicals within the sodalite β cages

[†] Weizmann Institute of Science.

[‡] Pennsylvania State University.

(1) Reinen, D.; Lindner, G.-G. The nature of chalogen colour centers in ultramarine-type solids. *Chem. Soc. Rev.* **1999,** *28,* 75–84.

(2) Vaughan, D. E. W.; Strohmaier, K. G.; Pickering, I. G.; George, G. N. Transition metal framework substitution in sodalites. *Solid State Ionics* **1992,** *55/56,* 1282–1291.

(3) http://www.iza-structure.org/databases/ModelBuilding/SOD.pdf.

(4) Barrer, B. M.; Vaughan, D. E. W. Trapping inert gases in sodalite and cancrinite. *J. Phys. Chem. Solids* **1971,** *32,* 731–743

(5) Tilley, R. J. D. *Colour and Optical Properties of Materials*; John Wiley and Sons: New York, 2000.

(6) Barrer, R. M. *Hydrothermal Chemistry of Zeolites*; Academic Press: London, 1982, and references therein.

(7) Gobeltz, N.; Demortier, A.; Lelieur, J. P.; Duhayon, C. Encapsulation of the chromophores into the sodalite structure during the synthesis of blue ultramarine pigments. *J. Chem. Soc., Faraday Trans.* **1998,** *94,* 2257–2260.

(8) Wieckowski, A. B.; Wojtowicz, W.; Sliwa-Niesclor, J. Temperature dependence of EPR linewidth of ultramarine blue. *Magn. Reson. Chem.* **1999,** *S37,* s150–s153.
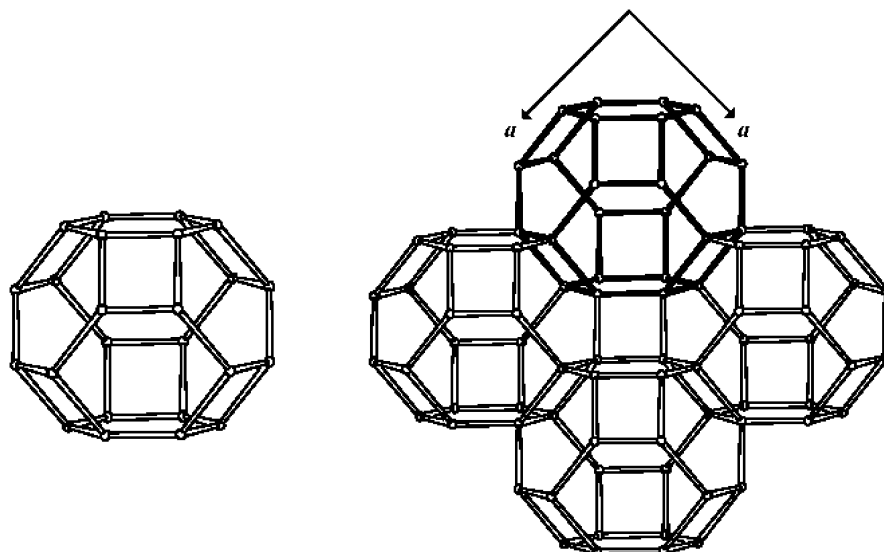
Figure 1. Structure of sodalite reproduced from the IZA website.[3] On the left the β-cage is shown, and on the right the structure of sodalite is depicted. The corners represent Si or Al connected via oxygen. The unit cell formula of the mineral sodalite is $Si_6 Al_6O_{24}Na_8Cl_2$.

readily explains their stability, despite the highly unstable di- and trisulfur radical anions.

In the past few decades, blue ultramarine pigments, characterized by high sulfur concentration, have become available commercially and were subjected to spectroscopic studies.[8−10] The industrial synthesis of these pigments consists of two steps. The first one, conducted in an inert atmosphere, involves heating a mixture of calcined kaolin, sulfur and a reducing agent, at about 1000 K and holding this temperature for a given period of time. The second step, performed after cooling to about 720 K, is oxidation with sulfur dioxide resulting from the reaction between the oxygen of the air and sulfur. In this work we present a new simple synthetic route in which the sulfur radicals are generated from reduction of sulfate anions, introduced into the synthesis gel, and trapped in the β cages, during calcination in air of as-synthesized sodalite. In this preparation aluminum sulfate serves as both the aluminum and the sulfur source, while tetramethylammonium ions are the source of reducing agents when decomposed at high temperatures. It is well known that when sulfate and tetramethylammonium ions are present, they occupy the center of the sodalite cages.[11]

The nature of the color species in blue ultramarine pigments and their identification as di- and trisulfur radical anions (S_2^- and S_3^-, respectively) have been the subject of a rather long and controversial history, which dates back to the early 1970s.[12] Experimental studies applying UV−vis, EPR, IR, and resonance Raman spectroscopy[13] as well as theoretical quantum mechanical

calculations[14] have all been used for identification and characterization. As a reference, earlier studies of impurity centers in sulfur-doped alkali halide crystals were used.[15−17] Since both S_3^- and S_2^- are paramagnetic, EPR has played a key role in these spectroscopic characterizations, and most experiments were performed in the continuous wave (CW) mode at X-band frequencies ($\nu_0 \sim 9$ GHz).[8,18]

CW EPR is a useful tool for determining the *g*-tensor components, as long as the *g* anisotropy is not too small, and for monitoring dynamic effects through temperature-dependent line shape variations. However, a detailed mapping of the close radical environment, particularly in disordered samples, can only be extracted from electron nuclear double resonance techniques (ENDOR) and/or electron spin−echo envelope modulation (ESEEM) experiments.[19] In general these techniques measure the nuclear frequencies (usually referred to as the NMR or ENDOR frequencies) of nuclei coupled by the hyperfine interaction to the unpaired electron. From these frequencies it is possible to extract the Larmor frequency and hyperfine interaction of the coupled nuclei. Once a coupled nucleus is identified by its Larmor frequency, its hyperfine interaction can be generally translated to geometrical parameters such as distance (2−6 Å) and orientation.

Earlier assignments of the different CW-EPR signals measured in synthetic blue sodalite pigments that originated from different sources were not fully consistent. Two "distinguishable" EPR signals were assigned to the S_3^- radical trapped in the sodalite cage. The most common one was an *isotropic* signal

(9) Eaton, G. R.; Eaton, S. S.; Stoner, J. W.; Quine, R. W.; Rinard, G. A.; Smirnov, A. I.; Weber, R. T.; Krzystek, J.; Hassan, A. K.; Brunel, L. C.; Demortier, A. Multifrequency electron paramagnetic resonance of ultramarine blue. *Appl. Magn. Reson.* **2001**, *21*, 563−570.

(10) Clark, R. J. H.; Dines, T. J.; Kurmoo, M. On the nature of the sulfur chromophores in ultramarine blue, green, violet, and pink and of the selenium chromophore in ultramarine selenium: characterization of radical anions by electronic and resonance Raman spectroscopy and the determination of their excited-state geometries. *Inorg. Chem.* **1983**, *22*, 2766−2772.

(11) Baerlocher, C.; Meier, W. M. Synthese und kristalstruktur von tetramethylammonuium-sodalith. *Helv. Chem. Acta* **1969**, *52*, 1853−1860.

(12) McLaughlan, S. D.; Marshall, D. J. Paramagnetic resonance of sulfur radicals in synthetic sodalites. *J. Phys. Chem.* **1970**, *74*, 1359−1363.

(13) Clark, R. J. H.; Cobbold, D. G. Characterization of sulfur radical anions in solutions of alkali polysulfides in dimethylformamide and hexamethylphosphoramide and in the solid state in ultramarine blue, green, red. *Inorg. Chem.* **1978**, *17*, 3169−3174.

(14) Koch, W.; Matterer, J.; Heinemann, C. Quantum chemical study on the equilibrium geometries of S_3 and S_3^-, The electron affinity of S_3 and the low lying electronic states of S_3^-. *J. Chem. Phys.* **1995**, *102*, 6159−6167.

(15) Schneider, J.; Dischler, B.; Räuber, A. Electron spin resonance of sulfur and selenium radicals in alkali halids. *Phys. Status Solidi* **1966**, *13*, 141−157.

(16) Suwalski, J.; Seidel, H. ENDOR investigation of the S_3^- sulfur centre in KCl and NaCl. *Phys. Status Solidi* **1966**, *13*, 159−168.

(17) Vannotti, L. E.; Morton, J. R. Paramagnetic resonance spectra of S_2^- in alkali halides. *Phys. Rev.* **1967**, *161*, 282−286.

(18) Gobeltz-Hautecoeur, N.; Demortier, A.; Lede, B.; Lelieur, J. P.; Duhayon, C. Occupancy of the sodalite cages in the blue ultramarine pigments. *Inorg. Chem.* **2002**, *41*, 2848−2854.

(19) Schweiger, A.; Jeschke, G. *Principles of Pulse Electron Paramagnetic Resonance*; Oxford University Press: Oxford, 2001.

characterized by $g = 2.029$, which remained isotropic even at liquid helium temperatures,[8,9,18] while in other studies the S_3^- was associated with a *rhombic g* tensor, for example, $g_{xx} = 2.005$, $g_{yy} = 2.036$, $g_{zz} = 2.046$.[12] The origin of the two different signals was explained by Gobeltz et al.[20] as the difference in the chemical environment of these species, and the isotropic signal was assigned to species, which are free to rotate at all temperatures. The EPR characteristics of the S_2^- impurities in alkali halides were detected only below 30 K and were characterized by a large g anisotropy (for example, in NaCl $g_{xx} = 2.2531$, $g_{yy} = 2.0107$, $g_{zz} = 1.9860$[21]). A broad EPR signal has been observed at room temperature in the spectrum of green ultramarine pigments and was previously assigned to S_2^-. However, later it was shown that this broad signal is due to an Fe^{3+} impurity.[22] The above inconsistencies regarding the properties of the S_3^- radicals in different samples can be resolved by the application of sophisticated EPR techniques, which will bridge the gap between the various assignments and in particular will explain the origin of the two signals ascribed to S_3^-. One way to relate the *g*-tensor components to a specific radical is the application of theoretical calculations, in particular by means of density functional theory (DFT).[23,24] This method is particularly suitable for small radicals comprised of light atoms. DFT predictions of *g*-tensors have recently gained considerable attention,[25-27] as they are significantly less demanding than the traditional (post Hartree–Fock) ab initio methods.

In this study we have prepared three blue pigments by a new method; calcination in air of sodalite samples synthesized with aluminum sulfate and an organic template, tetramethylammonium hydroxide. The new materials were structurally characterized by X- and W-band CW-EPR, X-band HYSCORE (hyperfine sublevel correlation spectroscopy[28]) and W-band pulsed ENDOR in combination with UV–vis spectroscopy. Each sample was prepared under different conditions (Al/Si ratio, calcination temperature), resulting in varying total and relative amounts of the various radicals. The interaction with the Na^+ ions was investigated through the ENDOR measurements, which resolved different environments for two S_3^- radicals associated with the same rhombic *g*-tensor. The interpretation of the EPR

Table 1. ICP Elemental Analysis, Given in Relative Molar Ratios, for the Three Ultramarine Pigments Investigated in This Work

sample	notation	color	Al/Si	Na/Si	S/Si	Fe/Si	calcination
blue sodalite I[a]	BS-I	blue	0.64	0.76	0.11	<0.003	893 K
blue sodalite II[a]	BS-II	deep blue	0.68	0.75	0.15	<0.003	1273 K
blue sodalite III	BS-III	light green	0.91	1.06	0.13	0.006	913, 1073 K

[a] From the same batch.

experiments and the assignment of the signals were aided by theoretical *g*-tensor calculations using DFT.

Experimental Section

Zeolite Synthesis. The sodalite samples I and II were made using the following gel composition: $1.1(TMA)_2O:1.45Na_2O:Al_2O_3:3.5SiO_2:120H_2O:0.9Na_2SO_4$. A total of 26.9 g of sodium silicate (PQ Corp, N-type), 31 g of 25% tetramethylammonium hydroxide (TMAOH) solution (Sachem), and 6 g of a seed solution (composition $16Na_2O:1.2Al_2O_3:15SiO_2:340H_2O$)[29] were mixed in a small blender. Then 17.8 g of sodium aluminate, dissolved in 25 g of water (doubly ionized), was added, followed by 15 g of $Al_2(SO_4)_3 \cdot 17H_2O$ (Aldrich). After homogenization, the fluid gel was transferred to 125 mL Parr Teflon lined autoclave and reacted at 453 K for 19 h. Then it was cooled to room temperature, vacuum filtered, washed on the filter with 500 g of deionized water, and dried in an air oven at 373 K. The seed solution is a highly basic cold aged sodium aluminosilicate solution containing colloidal sized "nuclei". It is used commercially to prepare faujasite and is known to accelerate the crystallization of several zeolites.[30] The sodium aluminate was made by reacting 18.9 g of Al_2O_3 (Alcoa C33) with 5 g of NaOH in 25 g of H_2O overnight in a Teflon jar, cooling the clear Al_2O_3 solution and adding 20.6 g of H_2O. The dried white sample was equilibrated for 3 days over a saturated $Ca(NO_3)_2$ solution (~50% RH) and a powder X-ray diffraction pattern was obtained between $2\theta = 4-50°$ (Siemens D500 X-ray diffractometer). It showed an excellent SOD diffraction pattern[31] with a unit cubic cell of 9.131 Å. (This is somewhat larger than previously reported for conventional TMA-SOD[11] and mineral SO_4-SOD.[32])

A modified gel composition was used for the preparation of sample III: $0.40(TMA)_2O:0.90Na_2O:Al_2O_3:2.51SiO_2:95H_2O:0.84Na_2SO_4$. A total of 52.8 g of sodium silicate, 31 g of 25% TMAOH solution, 6 g of seeds, and 48 g of water were mixed in a small blender. Then 17.8 g of sodium aluminate (EM Corp, Na/Al = 0.28, 11.4% H_2O) dissolved in 30 g of water was added, followed by 15 g of $Al_2(SO_4)_3 \cdot 9H_2O$ (VWR) dissolved in 20 g of water. After homogenization, the fluid gel was transferred to a 45 mL Parr Teflon lined autoclave and reacted at 423 K for 5 d. The sample exhibited a SOD structure with a cubic unit cell of 9.049 Å and a trace of LTA.[31] The sample was prepared for analysis in the manner described for samples I and II.

All samples were calcined in air as follows: sample I (blue sodalite I, BS-I) was calcined for 5 h at 893 K (cubic unit cell = 9.094 Å), sample II (blue sodalite II, BS-II) was calcined for about 1 h at 1273 K, and sample III (blue sodalite III, BS-III) was calcined first at 913 K for 3 h and then at 1073 K for 16 h. Table 1 presents the notation,[33] color, and chemical composition (relative molar percent) of the three samples, determined by ICP-AES analysis. TGA analysis in air of the zeolite prepared using the modified gel formulation (see above) showed a gradual water weight loss up to 550 °C (4%) and major losses at

(20) Gobeltz, N.; Demortier, A.; Lelieur, J. P.; Duhayon, C. Correlation between EPR, Raman, and colorimetric characteristics of the blue ultramarine pigments. *J. Chem. Soc., Faraday Trans.* **1998**, *94*, 677–681.
(21) Maes, F.; Matthys, P.; Callens, F.; Moens, P.; Boesman, E. EPR of S_2^- in RbCl and RbBr. *J. Phys.: Condens. Matter* **1992**, *4*, 259–256, and references therein.
(22) Gobeltz, N.; Demortier, A.; Lelieur, J. P.; Lorriaux, A.; Duhayon, C. Presence of Iron(III) impurities in ultramarine green pigments. *New J. Chem.* **1996**, *20*, 19–22, and references therein.
(23) Kohn, W; Becke, A. D.; Parr, R. G. Density functional theory of electronic structure. *J. Phys. Chem.* **1996**, *100*, 12974–12980.
(24) Koch, W.; Holthausten, M. C. *A Chemist's Guide to Density Functional Theory*; Wiley-VCH: Weinheim, 2000.
(25) Carl, P. J.; Isley, S. L.; Larsen, S. C. Combining theory and experiment to interpret the EPR spectra of VO^{2+}-exchanged zeolites. *J. Phys. Chem. A* **2001**, *105*, 4563–4573.
(26) Neese, F. Prediction of electron paramagnetic resonance g values using coupled perturbed Hartree–Fock and Kohn–Sham theory. *J. Chem. Phys.* **2002**, *115*, 11080–11096.
(27) Frantz, S.; Hartmann, H.; Doslik, N.; Wanner, M.; Kaim, W.; Kummerer, H. J.; Denninger, G.; Barra, A. L.; Toia, C. D.; Fiedler, J.; Ciofini, I.; Urban, C.; Kaupp M. Multifrequency EPR study and Density Functional g-tensor calculations of persistent organorhenium radical complexes. *J. Am. Chem. Soc.* **2002**, *124*, 10563–10571.
(28) Höfer, P.; Gropp, A.; Nebenführ, H.; Mehring, M. Hyperfine sublevel correlation spectroscopy: a 2D ESR investigation of the squaric acid radical. *Chem. Phys. Lett.* **1986**, *132*, 279–282.
(29) Vaughan, D. E. W.; Edwards, G. C.; Barrett, M. G. Synthesis of type Y faujasite. U.S. Patent 4,178,352, 1979.

(30) Vaughan, D. E. W. Secondary cation effects on sodium and potassium syntheses at Si/Al2 = 9: Pt.1-Phase Development in the Sodium System. *Mater. Res. Soc. Symp. Proc.* **1988**, *111*, 89–100 (Treacy. M. M. J., et al., Eds.).
(31) Treacy, M. M. J.; Higgins, J. B. *Collection of Simulated XRD Powder Patterns for Zeolites*, 4th ed.; Elsevier: Amsterdam, 2001.
(32) Barth, T. F. W. The structures of the minerals of the sodalite family. *Am. Mineral.* **1933**, *18*, 405–414.
(33) Although sample III appeared as a light green pigment, for consistency we use the notation blue-sodalite for all.
(34) Shane, J. J.; Gromov I.; Vega, S.; Goldfarb, D. A versatile pulsed X-band ENDOR spectrometer. *Rev. Sci. Instrum.* **1998**, *69*, 3357–3364.
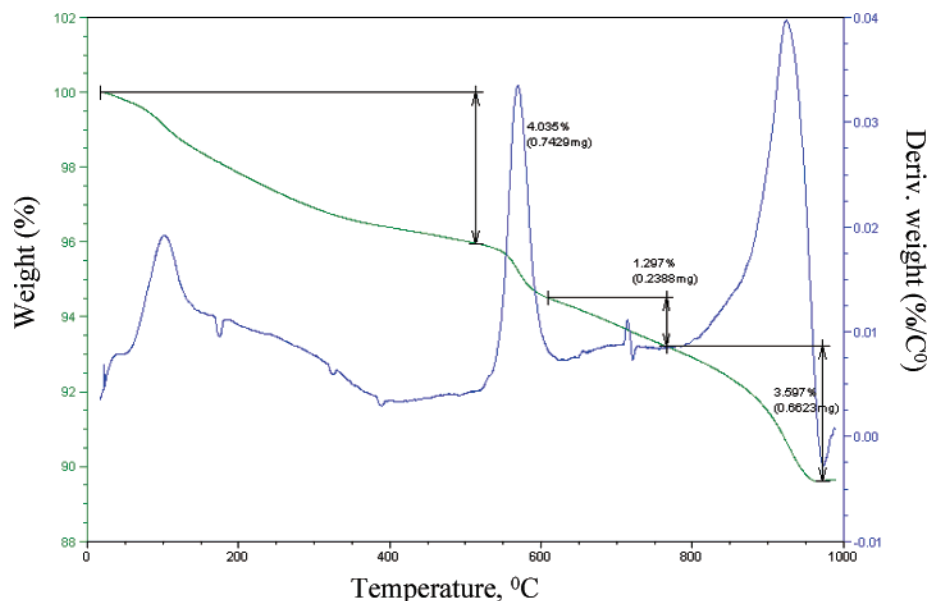
Figure 2. TGA analysis (in air) of the parent zeolite used to get BS-III upon calcination.

560−580 °C (1.7%) and 900−925 °C (3.6%). The first two peaks are attributed to TMA decomposition and the last one is probably associated with SO_4^{2-} decomposition (Figure 2).

The TGA sample at termination (1000 °C) was blue. However, examination of samples calcined in the muffle furnace showed that color development was time and temperature dependent (in addition to composition dependency). The initial white samples were white after calcination at 440 °C and turned black on TMA decomposition (600 °C); even after 3 h at 640 °C some samples were gray or gray-blue. In the absence of sulfate a TMA-SOD is white after 5 h at 640 °C. Subsequent heating at 800 °C for 18 h developed the blue and green colors. Samples placed in a muffle furnace at 1000 °C turned blue within 30 min. The development of color species is clearly dependent on several variables (T, t, dT/dt, O_2 presure, and chemical composition) including the presence of small amounts of transition elements that may catalyze the decomposition of the template. Preliminary TGA-MS experiments failed to define reaction product sequences, probably because of low concentrations of reaction products (apart from H_2O and CO_2). We have not analyzed the sampled for TMA^+ cations but their content can be estimated from the TGA and chemical analysis data of the calcined product given in Table 1. Assuming that all the S in the calcined sample originated from SO_4^{2-} and that no Na was lost in the calcination process, then for BS-III $TMA^+/Si = 2S/Si - (Na/Si - Al/Si) = 0.11$, which amounts to 4.6 wt % (not taking into account the water content). The weight loss due to TMA decomposition is about 3.4%, which is lower than the above estimate, indicating the presence of some residual carbon.

UV−Vis Measurements. UV−vis measurements were carried out at room temperature on a Varian Cary-300 Bio UV−vis spectrometer employing the diffuse reflectance mode. The samples were analyzed against a Labsphere Spectralon reflectance standard.

EPR Measurements. CW X-band EPR spectra were recorded on a Varian E-12 spectrometer (9.2 GHz) using a typical modulation amplitude of 0.1 mT at a frequency of 100 kHz. The X-band pulsed experiments were carried out both on a Bruker E-580 spectrometer at 9.5 GHz and temperature of 10 K and on a home-built spectrometer[34] at 8.5 GHz and 4.3 K. Field swept echo detected (FS-ED) spectra were recorded on the home-built spectrometer with the two-pulse echo sequence ($\pi/2-\tau-\pi-\tau$−echo) with $\pi/2$ and π pulses of 20 and 40 ns, respectively, and a repetition rate of 0.5 kHz. The HYSCORE spectra were measured using the four-pulse sequence ($\pi/2-\tau-\pi/2-t_1-\pi-t_2-\pi/2-\tau$−echo[29]) with $\pi/2$ and π pulses of 16 and 32 ns, respectively. The dwell time, Δt, was set to 32 ns, and the appropriate phase cycling

was employed.[35] The HYSCORE data were treated with the Bruker *Xepr* software as follows: the echo decay was removed from the time domain data by a polynomial fit and the resulting waveforms were apodized with a Hamming window function. Zero-filling up to 128/256 points was carried out, followed by a two-dimensional (2D) Fourier transformation and magnitude calculations.

W-band (94.9 GHz) CW and pulsed EPR spectra were recorded on a home-built spectrometer.[36] In the CW mode, field modulation at a frequency of 100 kHz and an amplitude of ∼1 mT was applied. The field was calibrated using a sample of ^{55}Mn/MgO, which was glued to one of the cavity flanges.[36] The pulsed experiments were carried out at a typical temperature of 5 K. FS-ED spectra were obtained using the two-pulse echo sequence with pulses of 60 and 100 ns, respectively. The Mims ENDOR experiments ($\pi/2-\tau-\pi/2-T-\pi/2-\tau$−echo, with an RF pulse applied during the time interval T[37]) were conducted with a $\pi/2$ pulse duration of 100 ns, and an RF pulse length (t_{RF}) of 15 μs. Davies ENDOR spectra ($\pi-T-\pi/2-\tau-\pi-\tau$−echo, with an RF pulse applied during T[38]) were obtained with $\tau = 400$ ns and two types of microwave pulses: "soft" pulses, where the π and $\pi/2$ pulse lengths were 200 and 100 ns, respectively, or "hard" pulses of 80 and 40 ns, respectively. The RF pulse length, t_{RF}, was set to 10 or 20 μs in the two types of Davies ENDOR experiments, respectively. To eliminate baseline distortions the RF frequency was varied randomly in all Davies ENDOR measurements.[39] The repetition rates were 0.2 kHz for the FS-ED and Mims ENDOR experiments and 0.1 kHz for the Davies ENDOR measurements. For convenience, the frequency scale in the ENDOR spectra is given relative to the ^{23}Na Larmor frequency, which is 38.24 MHz at $B_0 = 3.394$ T ($g{\sim}2$). The Mims ENDOR spectra were multiplied by (-1).

Geometry Optimizations. Gas-phase full geometry optimizations and energy calculations were carried out for the isolated sulfur radicals

(35) Fauth, J. M.; Schweiger, A.; Braunschweiler, L.; Forrer J.; Ernst, R. R. Elimination of unwanted echoes and reduction of dead time in three-pulse electron spin−echo spectroscopy. *J. Magn. Reson.* **1986**, *66*, 74−85.
(36) Gromov, I.; Krymov, V.; Manikandan, P.; Arieli, D.; Goldfarb, D. A W-Band pulsed ENDOR spectrometer: setup and application to transition metal centers. *J. Magn. Reson.* **1999**, *139*, 8−17.
(37) Mims, W. B. Pulsed ENDOR Experiments. *Proc. R. Soc. London* **1965**, *283*, 452−457.
(38) Davies, E. R. A new pulsed ENDOR technique. *Phys. Lett. A* **1974**, *47*, 1−2.
(39) Epel, B.; Arieli, D.; Baute, D.; Goldfarb, D. Improving W-band pulsed ENDOR sensitivity − random ENDOR and special TRIPLE. *J. Magn. Reson.* **2003**, *164*, 78−83.

with DFT,[23] using the Turbomole code Version 5.3.[40] The S_3^- species was optimized both under C_{2v} and D_{3h} point group symmetries, while no symmetry was employed for the S_2^- radical. The three parameters Becke exchange functional[41] and the Lee−Yang−Parr[42] correlation functional, i.e., the combination commonly denoted as B3LYP was employed, and a triple -ζ basis set enhanced with one polarization function was taken from Schäfer et al.[43] The cluster of S_3^- surrounded by four sodium cations, $[Na_4S_3]^{3+}$, was partially optimized under C_2 symmetry as follows: the geometry of the S_3^- radical as well as the positions of the cations were fixed, while the radical was free to move and rotate within these symmetry and ligands constraints. The following convergence criteria were used: 1E-6 Hartree for the energy change and 1E-3 Hartree/Bohr for the gradients. All three small sulfur radicals were also optimized using the gradient-corrected Becke exchange[44] and Perdew gradient corrected correlation functional,[45−47] denoted BP86, and the maximum differences in bond lengths and bond angles were 0.1 Å and 1°. We selected the structures obtained using the B3LYP functional rather than BP86 since the structures calculated with B3LYP were in better agreement with the structures reported in the literature using a post Hartree−Fock technique (CCSD(T)/ANO6532).[14]

DFT Calculations of *g*-Tensors. All-electron spin unrestricted Kohn Sham calculations of the *g*-tensor components were done using the ORCA code Version 2.2 developed by Frank Neese.[46]

The *g*-tensor was calculated as a correction to the free electron value, $g_e = 2.002319$, using perturbation theory:[26]

$$\mathbf{g} = g_e\mathbf{1} + \Delta\mathbf{g}$$

where $\Delta\mathbf{g}$ consists of several terms: (i) the relativistic mass correction, (ii) the diamagnetic correction, and (iii) the cross term between the orbital Zeeman and spin−orbit coupling operators. The first two terms are usually small and tend to cancel each other, while the last one is the dominant contribution.[26] We compared the performance of four different functionals: two pure DFT functionals (generalized gradient approximation, GGA), the BP86 described above and the BLYP functional, which combines the gradient-corrected Becke exchange[44] with the Lee−Yang−Parr[42] correlation functional, as well as two hybrid functionals, B3LYP, described above, and the PWP1 functional, which uses the Perdew−Wang gradient corrected exchange[45] together with Perdew's correlation functional.[47] Basis sets of Schäfer et al.[43] were employed as follows: for the sulfur atom a triple-ζ basis was enhanced with three polarization functions, while the core region was expanded by decontracting all *s* functions. For sodium we used a triple-ζ basis set enhanced with three polarization functions. Basis set convergence was verified for the S_3^- /C_{2v} radical. The calculations showed (relatively) little dependence on the functional; hence, we present in this paper only one set of results calculated using the BP86 functional. The complete basis set and functional studies are summarized in the Supplementary information.

(40) Ahlrichs, R.; Bär, M.; Häsner, M.; Horn, H.; Kölmel, C. Electronic structure calculations on work-station computers: the program system TURBO-MOLE. *Chem. Phys. Lett.* **1989**, *162*, 165−169.
(41) Becke, A. D. Density-functional thermochemistry. III. The role of exact exchange. *J. Chem. Phys.* **1993**, *98*, 5648−5652.
(42) Lee, C.; Yang, W.; Parr, R. G. Development of the Colle-Salvetti correlation-energy formula into a functional of the electron density. *Phys. Rev. B* **1988**, *37*, 785−789.
(43) Schäfer, A.; Horn, H.; Ahlrichs, R. Fully optimized contracted Gaussian basis sets for atoms Li to Kr. *J. Chem. Phys.* **1992**, *97*, 2571−2577.
(44) Becke, A. D. Density-functional exchange-energy approximation with correct asymptotic behavior. *Phys. Rev. A* **1988**, *38*, 3098−3100.
(45) Perdew, J. P.; Chevary, J. A.; Vosko, S. H.; Jackson, K. A.; Pederson, M. R.; Singh, D. J.; Fiolhais, C. Atoms, molecules, solids, and surfaces: applications of the generalized gradient approximation for exchange and correlation. *Phys. Rev. A* **1992**, *46*, 6671−6687.
(46) Neese, F. ORCA- an ab initio, DFT and semiempirical program package, Version 2.2−14; Universitat Konstanz: Konstanz, Germany, 2002. Un-published.
(47) Perdew, J. P. Density-functional approximation for the correlation energy of the inhomogeneous electron gas. *Phys. Rev. B* **1986**, *33*, 8822−8824.
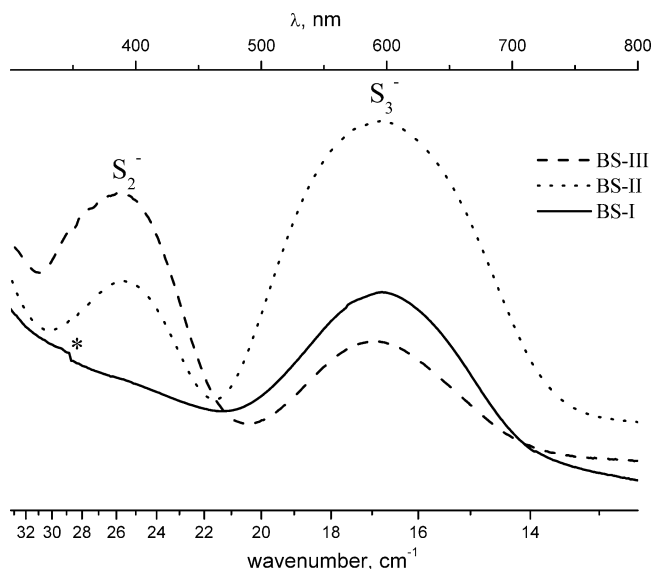
Figure 3. Powder UV−vis reflectance spectra (RT) of the three blue sodalite pigments.

Results

UV−Vis. The UV−vis spectra of the three blue sodalite samples are shown in Figure 3, and based on earlier literature reports we attribute the peaks at 595 and 395 nm to S_3^- and S_2^-, respectively.[48] The absorption below 350 nm is due to the sodalite framework superimposed on some instrumental baseline drift. A comparison between the spectra of BS-I and BS-II, both originating from the same parent sodalite sample, shows that the total radical amount $(S_2^- + S_3^-)$ is higher when the calcination is performed at a higher temperature and that the S_3^- radical is the first to form during the heating process. The final ratio between S_2^- and S_3^- depends, however, not only on the calcination procedure but also on the Al/Si ratio, as inferred from the strong S_2^- signal in the spectrum of BS-III.

CW EPR. The X-band spectra of BS-I (Figure 4a) are characterized by an anisotropic signal at both low and high temperatures (180 and 370 K, respectively); however, the anisotropy decreases with increasing temperature, indicating that some motional averaging takes place. The low-temperature X-band spectrum of BS-II (Figure 4b) exhibits features similar to those of the BS-I spectrum, with the exception that the center peak is significantly more intense. This indicates that the spectrum is a superposition of a well-defined powder pattern, similar to that exhibited by BS-I, and a broad singlet in the center. This is confirmed by comparison with the W-band spectra of BS-I (see below) where the singularities of the powder pattern do not overlap with the singlet. The presence of some motional averaging at room temperature is again evident from the broadening of the features corresponding to the powder pattern singularities. The spectrum of BS-III (Figure 4c) consists of a powder pattern and a superimposed isotropic signal, the relative intensity of which is significantly lower than that in BS-II. The temperature dependence of the powder pattern (not shown) is rather similar to that detected for BS-I. In addition, minute amounts of impurity signals are detected in the spectra of BS-I and BS-III. These minor species are probably organic

(48) Lindner, G.-G.; Massa, W.; Reinen, D. Structures and properties of hydrothermally synthesized thiosulfate cancrinite. *J. Solid State Chem.* **1995**, *117*, 386−391.
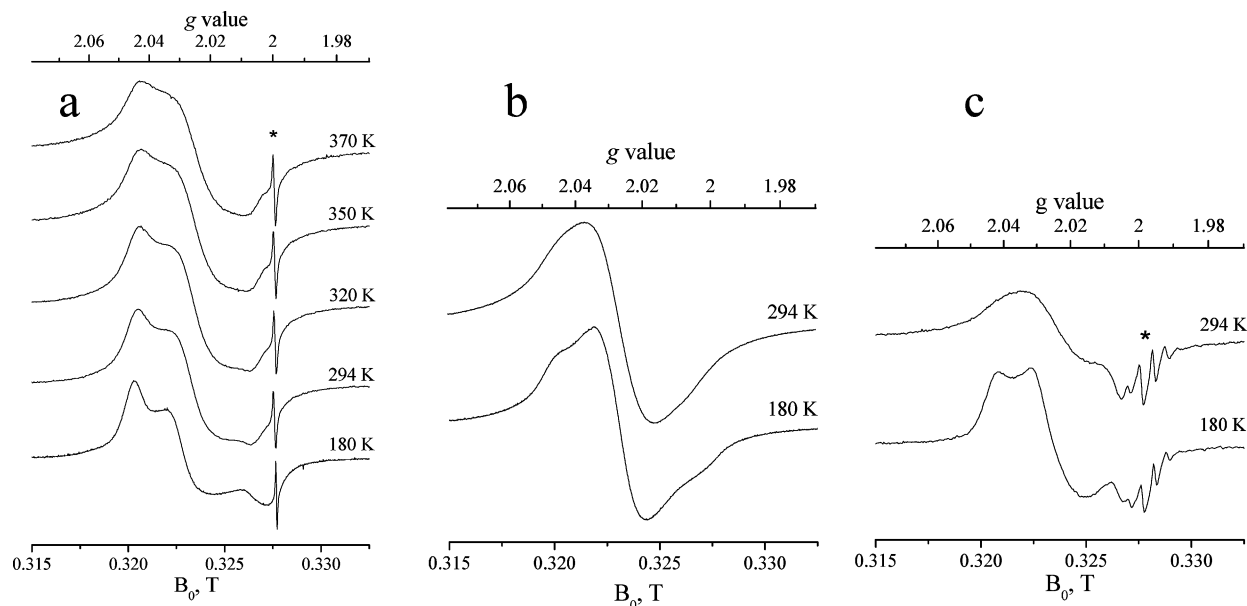
Figure 4. Variable temperature X-band CW EPR spectra of BS-I (a), BS-II (b), and BS-III (c). The asterisks mark impurity signals.
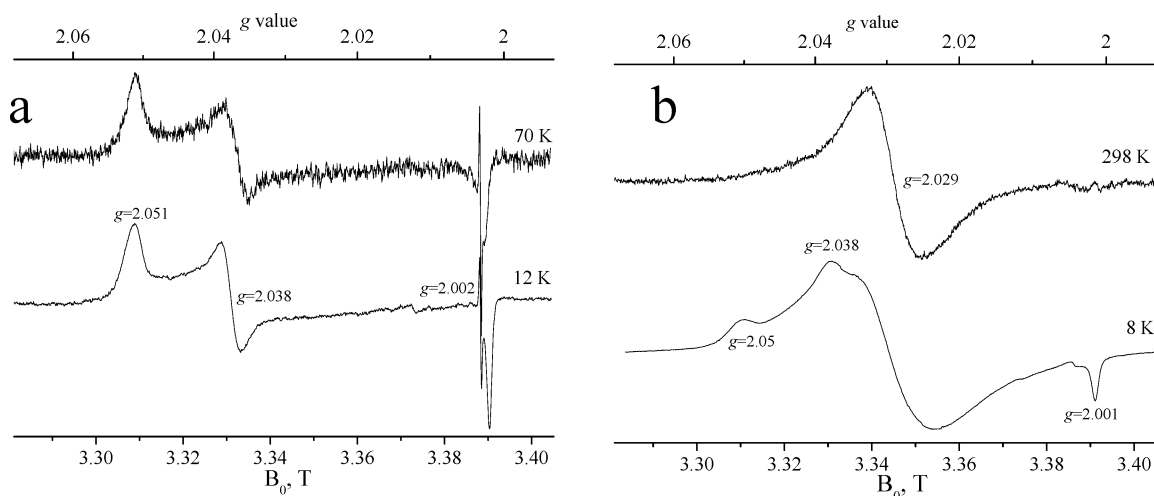

Figure 5. Variable temperature W-band CW EPR spectra of BS-I (a) and BS-II (b).

radicals (originating from the TMAOH) since their g values are very close to 2 and will not be discussed any further in this study.

To identify the source of the anisotropy in the spectra and determine more accurately the principal g values, spectra were recorded also at W-band (94.9 GHz). The low-temperature spectrum of BS-I (Figure 5a) shows a clear powder pattern, characteristic of a rhombic g-tensor with the principal values listed in Table 2. In contrast, the 8 K W-band spectrum of BS-II, shown in Figure 5b, is a superposition of two species; one with a rhombic g-tensor similar to BS-I, while the other has broad isotropic line with $g = 2.029$. The room-temperature spectrum of BS-I shows no signal, and comparison of the 12 and 70 K spectra (Figure 5a) shows a significant decrease in S/N, which indicates that the absence of the spectrum is due to sensitivity limitations of the spectrometer. Accordingly, the room-temperature spectrum of BS-II shows only isotropic signal (width of 120 G, compared with 21.3 G at X-band reported for an ultramarine blue sample with only an isotropic signal[9]). Reconstruction of the low-temperature spectrum of BS-II from its individual components (the room-temperature spectrum of

Table 2. Optimized Geometries and Calculated Principal g-Tensor Components for the Ground States of the S_3^- (Open and Closed Forms), S_2^-, and $[Na_4S_3]^{3+}$ Radicals along with the Experimental g-Values

species	sym	r, Å	α, deg	g_{xx}	g_{yy}	g_{zz}	g_{iso}
S_3^-	C_{2v}	2.06	114.9	2.061	2.039	2.002	2.034
S_3^-	D_{3h}	2.29	60.0	2.020	2.020	2.017	2.019
S_2^-	$D_{\infty h}{}^a$	2.06		2.858	2.034	2.002	2.298
$[Na_4S_3]^{3+}$	C_{2v}	2.68, 2.69, 2.84^b		2.064	2.042	2.002	2.035
BS-I (± 0.001)				2.051	2.038	2.002	2.030
BS-II^c (± 0.003)							2.029
BS-III (± 0.001)				2.050	2.037	2.001	2.029

^{a} The symmetry for S_2^-, $D_{\infty h}$, was not applied in the optimization and was replaced with no symmetry, C_1, to overcome problems of the Turbomole code in handling the high symmetry point group. ^{b} S$-$Na bond lengths. ^{c} Isotropic signal only.

BS-II and the low-temperature spectrum of BS-I) shows that the ratio between the isotropic and anisotropic signals is about 2:1.

Comparison of the line width of the isotropic signal of BS-II at X- and W-band shows that it increases with the applied
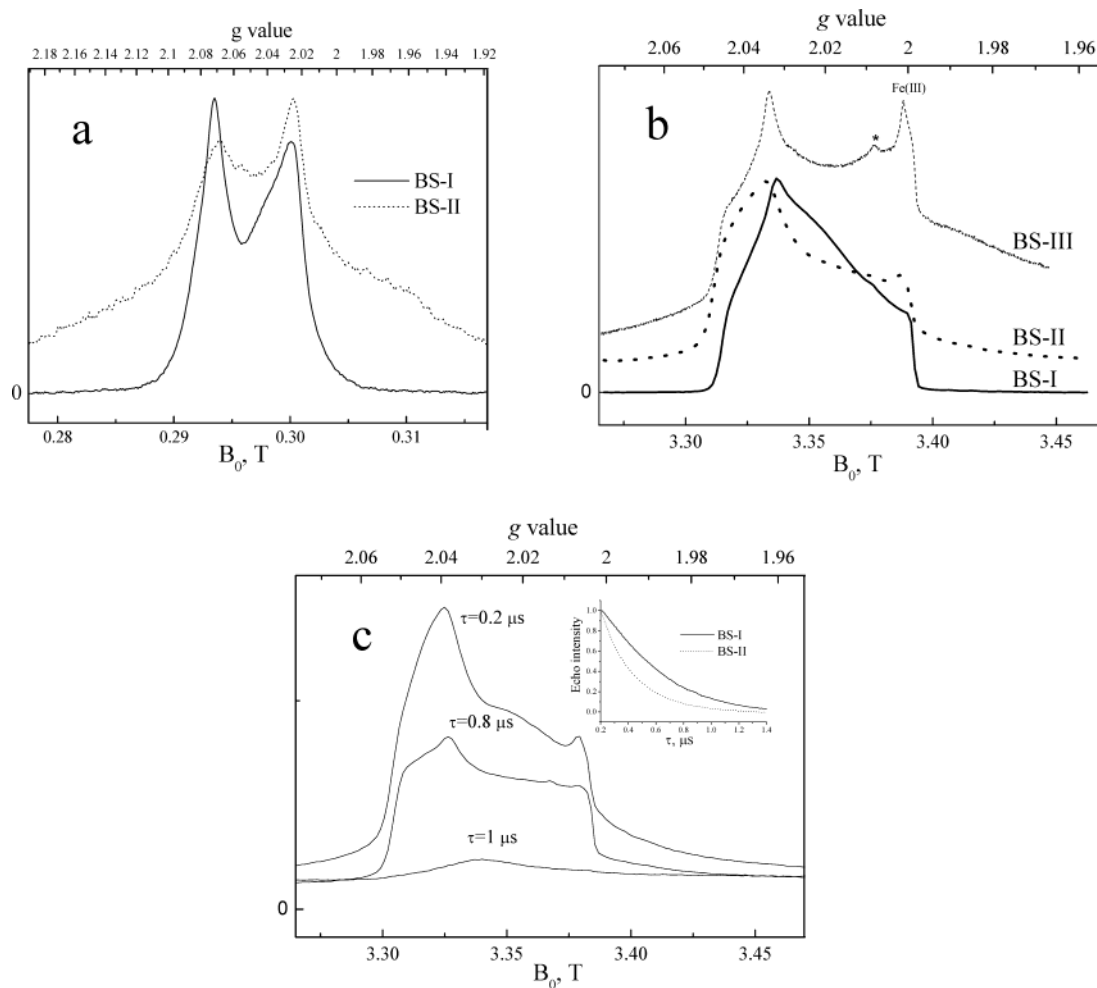
Figure 6. Low temperature (4−5 K) two-pulse FS-ED EPR spectra. (a) X-band spectra (τ = 270 ns) of BS-I and BS-II, (b) W-band spectra (τ = 500 ns) of the three pigments. The asterisk marks an impurity signal. (c) W-band spectra of BS-II using three different τ values and the two-pulse echo decay patterns of BS-I and BS-II at g = 2.038 are shown in the inset figure. In all graphs the baseline level is marked with "0".

magnetic field (compare Figures 4b and 5b). This is attributed to the presence of some residual g anisotropy and strain. The increase, however, does not scale linearly with the field, indicating that the broadening includes also field independent contributions. The W-band CW EPR spectrum of the green pigment (BS-III), recorded at 12 K, was very similar to that of BS-I, except for an additional impurity signal at $g \sim 2.0$, assigned to Fe^{3+} (data not shown). The high-spin Fe^{3+} signals are significantly narrow at W-band and therefore easily detected.[49] The presence of iron was later confirmed by chemical analysis, as presented in Table 1. The g-tensor components of the radical in BS-III, determined from the low-temperature measurements, are the same as for BS-I (see Table 2). To summarize, the CW EPR spectra reveal the presence of two types of radicals; one with an isotropic g-factor at all temperatures (down to 8 K) and a second one associated with a rhombic g-tensor. The sample calcined at the highest temperature, BS-II, shows the presence of both types, while the two samples calcined below 1100 K (BS-I and BS-III) show primarily presence of the radical characterized by the rhombic g-tensor.

On the basis of earlier reports[8,9,12,20] we assign both species to S_3^- radicals. This assignment is further substantiated by DFT calculations described later in this work.

FS-ED EPR. While the conventional method of measuring an EPR spectrum is CW-EPR, spectra can be also recorded in pulsed mode. There, a sequence which generates an echo is applied and the echo intensity is measured while sweeping the magnetic field, producing a so-called field sweep echo-detected EPR spectrum. Such a spectrum is in general similar to the absorption CW-EPR spectrum but is more sensitive to broad lines. In addition, species with different relaxation times can be distinguished through a proper adjustment of the repetition time of the experiment or the time interval between the pulses. FS-ED EPR spectra were recorded at a low temperature at X- and W-bands. X-band FS-ED EPR spectra of BS-I and BS-II (Figure 6a) exhibit a powder pattern in the range of g values determined from the CW EPR experiments, modified by the nuclear modulation effect.[50] The spectrum of BS-II is, however, superimposed on a broad background signal which is absent from the corresponding CW EPR spectra. Similar experiments carried out at W-band on the three different samples (Figure

(49) Arieli, D.; Vaughan, D. E. W.; Strohmaier, K. G.; Thomann, H.; Bernardo, M.; Goldfarb, D. Studies of Fe(III) Incorporated into AlPO4-20 by X- and W-band EPR Spectroscopies. *Magn. Reson. Chem.* **1999**, *37*, S43−S54.

(50) Goldfarb, D.; Kevan, L. Effect of nuclear modulation on field-swept electron spin−echo spectra. *J. Magn. Reson.* **1988**, *76*, 276−286.

6b) exhibit the same features scaled by the magnetic field. At high fields the nuclear modulation effect usually vanishes and the line shape of the FS-ED EPR spectrum is more similar to that of the CW EPR spectrum. The spectra are predominantly anisotropic, implying that the component with the isotropic *g*, which dominates the CW EPR spectra of BS-II, has only a little (if any) contribution. This, in turn, indicates that the species with the isotropic *g* has a significantly shorter relaxation time. The spectrum of BS-III also exhibits a clear background signal throughout the field range scanned. In this particular case, however, part of this signal, particularly at *g* < 2, is due to the Fe^{3+} impurity signal. These large background signals in BS-II and BS-III correlate with the strong signals of S_2^- in their UV−vis spectra (Figure 3), suggesting that the background EPR signal is due to S_2^-. Its width is, indeed, consistent with its large *g* anisotropy in alkali halide defect sites (1.29 < *g* < 3.36[21]). Additional FS-ED measurements on BS-II with different *τ* values indicate that the line shape is strongly *τ* dependent (Figure 6c). The nuclear modulation effect can explain the small variations between the upper two spectra;[50] however, the spectrum measured with *τ* = 1 *μ*s shows a significantly different line shape. This indicates that the species contributing to the spectrum have significantly different phase memory times and therefore their relative contributions to the spectrum is strongly *τ* dependent leading to changes in the line shape. As the reduction in the background signal with increasing *τ* is small, we attribute the residual signal detected at *τ* = 1 *μ*s to the contribution of S_2^-, with the maximum intensity corresponding to g_{yy}. The latter assignment will also be verified by the DFT calculations.

Two-pulse echo decay patterns were measured for BS-I and BS-II at the three canonical orientations, and no anisotropy was detected at 5 K. There was, however, a difference in the relaxation behavior in the two samples; the phase memory time, T_M, was found to be significantly shorter for BS-II, as shown in the inset of Figure 6c. Moreover, the apparent spin−lattice relaxation rate was also significantly faster, preventing ENDOR measurements (see below). This is attributed to extensive spectral diffusion due to the larger amount of paramagnetic species in this sample, in accordance with the integrated signal intensities found in the CW EPR and UV−vis spectra.

ENDOR. In pulsed ENDOR a pulse sequence generating an electron-spin−echo is applied, whereby an RF pulse on resonance with one of the NMR transitions induces a change in the echo intensity due to transfer of populations between the energy levels. The most commonly applied pulse ENDOR sequences are the Davies[38] and Mims[37] experiments. Reviews on pulsed ENDOR techniques and their applications are found in refs 51−53. To first order and for a weak coupling, which often applies to W-band frequencies, the two ENDOR frequencies for an unpaired electron, *S* = 1/2 (M_S = ± 1/2) coupled to a nuclear spin *I*, are given by[19] $ν_{α,β} = ν_I − M_S A$, $ν_I$ is the nuclear Larmor frequency and *A* is the hyperfine coupling. The nuclear quadruple interaction for *I* ≥ 1 has been neglected in the above.

(51) Gemperle, C.; Schweiger, A. Pulsed electron-nuclear double resonance methodology. *Chem. Rev.* **1991**, *91*, 1481−1505.
(52) Grupp, A.; Mehring, M. Pulsed ENDOR spectroscopy in solids. In *Modern Pulsed and Continuous-Wave Electron-Spin Resonance*; Kevan, L., Bowman, M. K., Eds. J. Wiley & Sons: New York, 1990; pp 195−230.
(53) Thomann, H.; Bernardo, M. Pulsed electron−nuclear multiple resonance spectroscopic methods for metalloproteins and metalloenzymes. *Methods Enzymol.* **1993**, *227*, 118−189
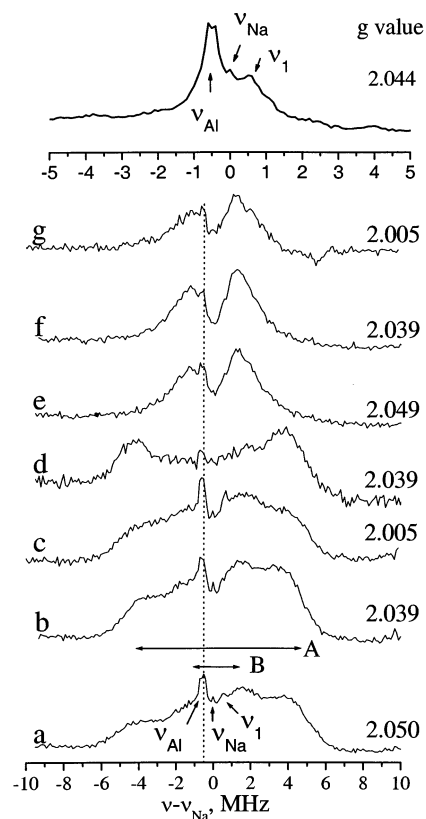
Figure 7. W-band ENDOR spectra of BS-I and BS-III. Top: Mims ENDOR spectra measured on BS-I with *τ* = 200 ns. Bottom: Davies ENDOR spectra recorded for BS-I (a−d) and BS-III (e−g) at the three canonical orientations. In all traces $t_π$ = 200 ns, except trace *d* for which $t_π$ = 80 ns. The "strong" and "intermediate" ^{23}Na hyperfine couplings are marked on trace *a* with "A" and "B", respectively, while the dotted line indicates $ν_{Al}$.

We have carried out W-band ENDOR measurements to get more insight into the structures of the radicals identified in the EPR spectra, in particular, to explore their interaction with the sodalite framework. Figure 7 shows an example of the Mims ENDOR spectrum of BS-I (top trace) recorded at *g* = 2.044. It exhibits three narrow peaks; two of them appear at the Larmor frequencies of ^{27}Al and ^{23}Na, $ν_{Al}$ and $ν_{Na}$, respectively, while the third line, denoted "$ν_1$", appears at $ν_{Na}$ + 0.5 MHz. Because $ν_{Al}$ is shifted with respect to $ν_{Na}$ by −0.5 MHz, we attribute the strong peak at $ν_{Al}$ to a superposition of a matrix ^{27}Al line and the low-frequency component of a ^{23}Na doublet with |*A*| = 1 MHz. Additional Mims ENDOR spectra recorded at different fields within the EPR spectrum show the expected field dependence (data not shown), thus supporting this assignment.

Davies ENDOR spectra of BS-III recorded with selective MW pulses ($t_π$ = 200 ns) (Figures 7e−g) show a doublet with a splitting of 2.6 ± 0.2 MHz, in addition to the three peaks detected in the Mims spectrum of BS-I. This doublet is attributed to ^{23}Na on the basis of the position of its center, which is closer to $ν_{Na}$ than to $ν_{Al}$. Moreover, it is more likely that Na^+ cations are in close contact with the anionic S_3^- radical rather than the negatively charged framework Al sites. The line shape and the weak orientation dependence of this signal indicate that the ^{23}Na hyperfine interaction is primarily isotropic and that the anisotropy is contained within the line width. The corresponding ENDOR spectra of BS-I (traces a−c) are characterized by a much broader signal centered around $ν_{Na}$ with a similar weak

orientation dependence. A comparison between the Davies spectra of BS-III and BS-I shows that the spectrum of the latter sample is a superposition of two broad and predominantly isotropic ^{23}Na doublets, one with a hyperfine splitting of 8 ± 1 MHz, marked as doublet "A" in Figure 7a and the other with 2.6 ± 0.4 MHz, marked as "B", already observed in BS-III. The narrow signals detected in the Mims ENDOR spectra are present in all spectra, although with a reduced intensity, attributed partially to the lower sensitivity of Davies ENDOR to small couplings. Davies ENDOR spectra recorded with shorter MW pulses (trace d) show only the doublet with the 8 MHz splitting. The Davies ENDOR spectra of BS-I are somewhat asymmetric with respect to the intensities of the doublet components. The source of the asymmetry is not fully clear. We have verified that it is neither a consequence of the saturation of the NMR transitions[54−62] nor a strong frequency dependence of the RF field strength. The large line width of the ^{23}Na doublets ($\sim$1.5 MHz and $\sim$2 MHz) is most probably due to unresolved nuclear quadrupole splittings, hyperfine anisotropy, and possibly also some A-strain. Unfortunately, we could not perform ENDOR experiments on BS-II due to its fast echo decay.

To summarize, the ENDOR experiments reveal the presence of three types of ^{23}Na nuclei: (a) those with strong coupling $\langle A_{\mathrm{iso2}} \rangle = 8 \pm 1$ MHz, (b) those with an intermediate coupling, $\langle A_{\mathrm{iso1}} \rangle = 2.6 \pm 0.2$ MHz, and (c) weakly coupled ^{23}Na nuclei with $|A| \sim 1$ MHz. Finally, remote ^{23}Na and ^{27}Al nuclei with signals at the corresponding Larmor frequencies are present as well. Despite the close similarity between the g values of the S_3^- radicals in BS-I and BS-III, their immediate environment are different, as BS-I shows interaction with all types of ^{23}Na while in BS-III only ^{23}Na ligands of types (b) and (c) are present.

HYSCORE. All ESEEM experiments involve the application of a series of microwave pulses which produce an electron spin−echo, the intensity of which is measured as a function of one of the pulse intervals.[54] This generates an echo decay envelope that is modulated when the unpaired electron experiences an anisotropic hyperfine interaction with nearby nuclei.[19] The modulation frequencies are the ENDOR frequencies. ESEEM experiments are usually sensitive to weak hyperfine interactions

Figure 8. X-band HYSCORE spectra measured for BS-I and BS-II at $g_{xx} = 2.051$ applying $\tau = 90$ ns.

($<$6 MHz) and the modulations are best detected at low fields (usually X-band and below). One of the most useful ESEEM experiment is the two-dimensional (2D) hyperfine-sublevel correlation experiment, termed HYSCORE.[29] The HYSCORE experiment provides 2D spectra with cross-peaks that represent correlations between the ENDOR frequencies of one electron spin manifold with the nuclear frequencies of the other electron spin manifold. For example for $S = 1/2$, $I = 1/2$, the cross-peaks appear at (ν_α, ν_β) and (ν_β, ν_α). This experiment is most useful for the assignment of ESEEM signals and for the detection of broad signals which are absent from the ESEEM spectrum due to the spectrometer dead time.[55,56]

ENDOR measurements could not be carried out on BS-II because of its fast echo decay, which did not allow for the introduction of an RF pulse. Hence, the HYSCORE technique was used. We have succeeded to measure HYSCORE spectra of BS-II only with very short τ values ($\lesssim$130 ns) and for comparison also the spectrum of BS-I was measured under similar conditions. Figure 8 presents the X-band HYSCORE spectra measured at $g_{xx} = 2.051$ with $\tau = 90$ ns for both samples. HYSCORE experiments at g_{yy} and g_{zz} were similar to the spectra recorded at g_{xx}, thus showing no orientation dependence (not shown). The spectrum of BS-I shows a ridge centered at $\nu_{\mathrm{Na}}(\nu_{\mathrm{Al}})$ with a maximum spread corresponding to $A = 4.5$ MHz. These results show that the HYSCORE measurements failed to detect the large ^{23}Na doublet ($\langle A_{\mathrm{iso2}} \rangle = 8 \pm 1$ MHz) observed in the W-band ENDOR spectra. The spectrum of BS-II is significantly different and shows a peak on the diagonal at $\nu_{\mathrm{Na}}(\nu_{\mathrm{Al}})$. We attribute the spectral differences between the two samples to considerable contributions from S_2^- which is not present in BS-I. The absence of cross-peaks in the spectrum of BS-II suggests that the S_2^- radical has weaker interactions with ^{23}Na as compared to the sulfur radical in BS-I. However, since we cannot resolve the ^{27}Al and ^{23}Na frequencies at this field,

(54) Deligiannakis, Y.; Louloudi, M.; Hadjiliadis, N. Electron spin−echo envelope modulation (ESEEM) spectroscopy as a tool to investigate the coordination environment of metal centers. *Coord. Chem. Rev.* **2000**, *204*, 1−112.

(55) Shane, J., J.; van der Heijden, P. A. A. W.; Reijerse, E. J.; de Boer, E. An ESEEM investigation of single crystals and powders of copper-doped L-histidine hydrochloride monohydrate. *Appl. Magn. Reson.* **1994**, *6*, 427−454.

(56) Kofman, V.; Shane, J. J.; Dikanov, S. A.; Bowman, M. K.; Libman, J.; Shanzer; A.; Goldfarb, D. Coordination of Cu(II) to lipophilic bis-hydroxamate binders as studied by one- and two-dimensional electron spin−echo spectroscopy. *J. Am. Chem. Soc.* **1995**, *117*, 12771−12278.

(57) Wirnsberger, G.; Fritzer, H. P.; Van de Goor, G.; Pillep, B.; Behrens, P.; Popitsch, A. Spectroscopic investigations of novel host−guest compounds based on microporous SiO$_2$ frameworks and inorganic guest species. *J. Mol. Struct.* **1997**, *410−411*, 123−127.

(58) Shah, R.; Payne, M. C.; Lee, M.-H.; Gale, J. D. Understanding the catalytic behavior of zeolites: a first-principles study of the adsorption of methanol. *Science* **1996**, *271*, 1395−1397.

(59) Lons, V. J.; Schultz, H. Strukturverfeinerung von Sodalith, Na$_8$Si$_6$Al$_6$O$_{24}$-Cl$_2$. *Acta Crystallogr.* **1967**, *23*, 434−436.

(60) Molin, Y. N.; Salikhov, K. M.; Zamaraev, K. I. Spin exchange. Principles and applications in chemistry and biology. In *Springer Series in Chemical Physics*; Goldanskii, V. I.,; Gomer, R., Schäfer, F. P., Toennies, J. P., Eds.; Springer-Verlag: Germany, 1980.

(61) Wieckowski A. Ultramarin study by EPR. *Phys. Status Solidi* **1970**, *42*, 125-&.

(62) Epel, B.; Poppl, A.; Manikandan, P.; Vega S.; Goldfarb, D. The effect of spin relaxation on ENDOR spectra recorded at high magnetic fields and low temperatures. *J. Magn. Reson.* **2001**, *148*, 388−397.
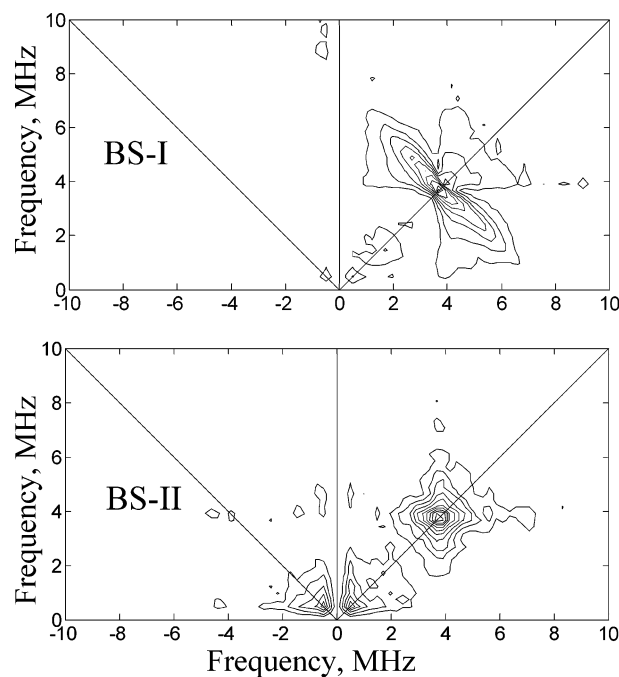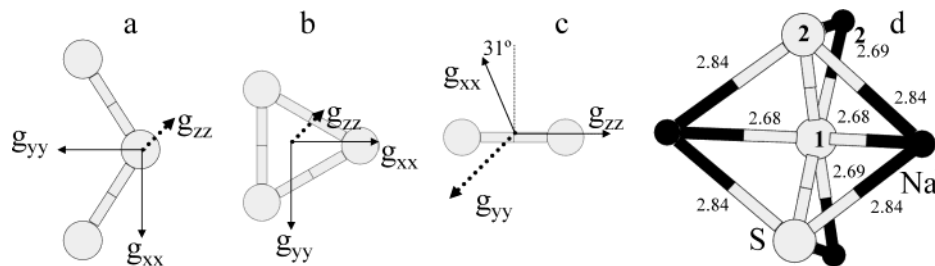
Figure 9. Optimized geometries used for the *g*-tensor DFT calculations: (a) S_3^- optimized under C_{2v} symmetry, (b) S_3^-/D_{3h}, (c) S_2^-/C_1, and (d) $[Na_4S_3]^{3+}/$ C_{2v}. The calculated *g*-tensor orientations and the S−Na bond lengths (Å) in the cluster are marked as well.

the possibility that the HYSCORE signal of BS-II is due to interaction with ^{27}Al cannot be ruled out.

DFT Calculations of the *g*-Tensor Components. To substantiate the assignment of the EPR signals, particularly those with isotropic and anisotropic *g*, to specific S_3^- radicals, the *g*-tensors of a few optimized clusters were calculated using DFT. Table 2 presents the experimental *g*-tensor components of the various species along with the corresponding calculated values for four optimized radical structures. The latter were selected according to literature reports discussed in the Introduction. These structures, as well as the *g*-tensor orientations, are schematically displayed in Figure 9. The S_3^- radical can appear either in an open (C_{2v}) or a closed (D_{3h}) form, where the gas-phase energy of the open form was found to be 43.3 kcal/mol lower than the closed one. Koch and co-workers have studied the relative stability of these two forms employing post-Hartree−Fock techniques (coupled cluster and second-order multireference perturbation theory) and obtained very similar results,[14] thus providing a good support for our DFT approach. The thermal energy, *kT*, at the calcination temperatures is about 2 kcal/mol, much smaller than the energy gap between the two conformations; nonetheless, because the interaction with the zeolite can alter this gap,[57,58] we chose to include also the closed form in our calculations. The fourth row in Table 2 presents calculations on a cluster model of S_3^- interacting with Na^+ cations.

The calculations on the three isolated radical species indicate that the species with the anisotropic *g* is most likely S_3^-/C_{2v}. The closed form has an axially symmetric *g*-tensor with only a slight anisotropy, whereas the S_2^- species has an extremely large *g* anisotropy, in agreement with the data available for alkali halide impurities.[17,21] The broad background signal in the FS-ED spectra of BS-II and BS-III fits the range of *g* values calculated for S_2^-, assuming that the experimental line width at g_{zz} is broad. This is a reasonable assumption considering the fact that it could not be detected in the CW EPR spectra. Moreover, the maximum signal detected in the FS-ED spectrum of BS-II at $\tau = 1$ μs (Figure 6c) is centered at $g \sim 2.03$, which is in good agreement with the calculated g_{yy} of S_2^-. The similarity between the *g* value of the isotropic signal and the calculated g_{iso} for the S_3^-/C_{2v} suggests that it may originate from the same S_3^- radical but in a different environment, which allows free rotation at all temperatures. Alternatively, some of the S_3^- species in BS-II may be in close proximity, for example, radicals located in neighboring cages, such that the spin−spin interaction becomes substantial, leading to exchange narrowing. The latter was already suggested by Eaton et al.,[9] and these two options are further discussed in the next section.

The *g* anisotropy predicated for the closed form of S_3^- is very small and at W-band the width of the powder pattern should be 5 mT, which is smaller than the width of the isotropic line (12 mT). This may suggest that the isotropic signal is due the closed form of S_3^-. We exclude this possibility on the basis of the predicted g_{iso} value, 2.019 for the closed form, compared to 2.034 for the open form. The latter is closer to the experimental value, 2.029, of the isotropic signal. The difference between the predicted values of the two forms amounts to 244 G, which is significantly larger than the line width of the isotropic signal. The differences are also significant in terms of the DFT calculation accuracy. Calculations of the *g*-tensor using different functionals and basis sets for the open form of S_3^- gave a maximum deviation of ± 0.02 for g_{iso} (see Supporting Information).

In a recent publication, Gobeltz-Hautecoeur et al.[18] have measured an isotropic signal for a blue ultramarine pigment and suggested that the S_3^- color center is located in the center of the sodalite β cage. Given a composition of $[Al_3Si_3O_{12}]Na_3$ (Al/ Si = 1), and an additional Na^+ to balance the radical charge, the radical is surrounded by four Na cations in each cage, situated 3−4 Å away from the sulfur atoms.[18] We have explored this suggestion by optimizing a cluster consisting of the S_3^-/C_{2v} radical surrounded by four Na^+ ions (namely, $[Na_4S_3]^{3+}$) and calculated the corresponding *g* values and spin density distribution by means of DFT. The ions were placed in their cationic positions, as determined by X-ray diffraction,[59] and the optimization allowed only the S−Na distances to vary.

The *g*-tensor components of the optimized complex (Table 2) are slightly larger than the bare radical; however, the agreement with the experimental data (anisotropic *g*) is still satisfactory. The $[Na_4S_3]^{3+}$ cluster contains two distinguishable sulfur and sodium atoms, whose identification as "1" and "2" is marked on Figure 9. Unlike the calculated *g* values which showed a small variation with respect to the functional used, the calculated spin densities and ^{23}Na hyperfine constants obtained using the four different functionals, described in the Experimental Section, showed a strong dependence on the type of functional chosen for $^{23}Na(1)$. For example, hybrid functionals predicted $A_{iso} < 1$ MHz while pure DFT functionals predicted $A_{iso} \approx 3-4$ MHz. In contrast, for $^{23}Na(2)$, all four functionals predicted $A_{iso} \approx -(2-2.5)$ (data not shown). Due to the relatively large variation for $^{23}Na(1)$ we have decided, for the time being, not to continue with the calculations of the hyperfine values and did not check other structures.

Discussion

Signal Assignment and Radical Characterization. While the EPR spectra clearly indicate the coexistence of S_3^- radicals

Table 3. Estimations of the Percentage (%) of β Cages Occupied with the Various Sulfur Anions in the Blue Sodalite Samples Investigated Obtained from the Chemical Analysis Data

sample	S_3^-(max) = Na_{ex}^+	S_3^- (if were the only anion)	S_3^-	S_2^-	SO_4^{2-}	SO_4^{2-} before calc.[b]	TMA^+ before calc.[b]
BS-I	44%	13.3	7.2		17.9	40	36
BS-II[a]	25%	17.8	15.8	4.8	4.1	53.5	82
BS-III	50.4%	13.7	7.35	13.7	13.8	41	31

[a] The chemical analysis has a large error, probably in the S content and maybe also in the Al, which results in a total SO_4^{2-} and TMA^+ occupancy larger than 100%. [b] Calc. = calcination.

in two different environments, their UV−vis signals are nearly identical. A close inspection of the UV−vis spectra (Figure 3) shows, however, that the S_3^- peak is somewhat broader in the spectrum of BS-II as compared to BS-I, thus suggesting contributions from two distinguishable types of S_3^-. The combination of CW and pulsed EPR with theoretical *g*-tensor predictions lead to the conclusion that the calcination below 1100 K (BS-I, BS-III) results in the formation of the S_3^- radical in an open form (C_{2v}) characterized by a rhombic *g*-tensor, the motion of which is strongly hindered even at 370 K. This indicates that this radical is strongly bound to the sodalite framework through the ^{23}Na ions, as confirmed by the substantial ^{23}Na hyperfine couplings. Calcination around 1300 K (BS-II) generates the second type of S_3^- species (also C_{2v}), characterized by an isotropic *g* at all temperatures down to 8 K. The isotropic *g* value is the same as g_{iso} of the anisotropic *g* tensor.

Two mechanisms can explain the isotropic signal: (i) Hopping between multiple orientations with respect to the external field. Since two of the *g*-tensor components (g_{xx}, g_{yy}) are within the molecular plane, while the third component (g_{zz}) is oriented perpendicular to this plane (Figure 9), the hopping between different orientations cannot be restricted to the molecular plane, which seems unlikely at 5 K. (ii) Spin exchange[9,60] between neighboring S_3^- radicals. This situation is likely to occur when the radical concentration is relatively high, such that several neighboring β cages can be occupied with radicals. In this case the closest distance of interaction is equivalent to the center-to-center distance of neighboring cages, ∼9 Å, which will induce strong spin−spin interaction. This in turn averages the *g* anisotropy, thereby generating an exchange narrowed signal.[9] Furthermore, the strong spin exchange leads to short echo decays, which prevented the observation of this sulfur radical in the pulsed EPR experiments. The isotropic signal with a Lorentzian line shape has been previously assigned to S_3^- radicals are arranged on a face centered cubic lattice with a constant of 18 Å.[61]

An estimate regarding the percentage of β cages occupied by S_3^- radicals and their distribution can be obtained from the chemical analysis data presented in Table 1. The ideal chlorosodalite formula, $Si_{12-x}Al_xO_{24}Na_{x+2}Cl_2$, implies that for a full occupation with S_3^- S:(Si + Al) = 1/2, which is far above the ratio detected by ICP (Table 1) for any of the samples. Moreover, for a complete occupation, the content of the extra Na^+, Na_{ex}^+ (beyond that required to balance the framework Al charge), should be Na_{ex}^+:(Al + Si) = 1/6. Hence, the content of Na_{ex}^+, given by Na/Si−Al/Si, provides an upper limit to the % of cages occupied with S_3^-, referred to as S_3^-(max). Table 3 lists the S_3^-(max) values for BS-I, II, and III. The difference between BS-I and BS-II is attributed to the experimental error

since the Al/Si ratio in both samples should be identical as they originate from the same batch (see Table 1). It is also possible that some dealumination takes place during the calcination, but in this case for differences to occur some of the dealuminated Al must be washed out. On the other hand if we assume that all the sulfur is present as S_3^-, this would account only for 13.3%, 17.8%, and 13.7% of the cages for BS-I, II, and III, respectively. These numbers are significantly smaller than the percentage of filled cages obtained from the Na_{ex}^+ content. Since the Na_{ex}^+ charge has to be balanced, many cages must still be occupied with SO_4^{2-} that has not been reduced and/or S_2^-. In the case of BS-I, which does not contain any S_2^-, it is possible to calculate the relative amount of S_3^- and SO_4^{2-} and to obtain the % of cages they occupied. This yields 7.2% for S_3^-, which is rather a low occupancy and is consistent with the a spectrum of isolated S_3^- radicals exhibiting an anisotropic powder pattern with no indication of spin exchange. From the chemical analysis and charge balance consideration it is possible also to estimate the number of cages occupied with TMA^+ and SO_4^{2-} before the high temperature calcination, assuming that the only anion present is SO_4^{2-} (TMA^+/Si = 2S/Si − (Na/Si − Al/Si), see Experimental Section). Table 3 lists the values obtained for the three samples. While for BS-I and BS-III the numbers make sense, for the case of BS-II we get an occupation of TMA^+ + SO_4^{2-} larger than 100% which is not realistic, since one cage cannot occupy both. This is attributed to the experimental error, mainly overestimation of the S content, and maybe also in the Al, which should be similar to that of BS-I.

The main difference between BS-I and BS-III is the substantial amount of S_2^-. The relative occupancy of the β cages with S_3^-, S_2^-, and SO_4^{2-} in BS-III can be obtained under the assumption that the absorbance coefficient of the two radicals is the same. Thus, their relative amounts can be determined from the relative intensities of the peaks at 595 and 395 nm in the UV−vis spectrum (Figure 3). The S_3^- occupancy is similar to that of BS-I, but there is a significant occupancy of S_2^- which can also contribute to the spin−spin interactions or lead to some clustering of the S_3^- and to the presence of an isotropic line. Although the numbers obtained for BS-II are not as reliable, it is still clear that it has the highest content of S_3^- from the UV−vis spectrum attributed to a larger degree of reduction of SO_4^{2-} by the TMA^+ due to the higher calcination temperature. The cage occupations listed in Table 3 for BS-II can be considered as an upper limit for S_3^- occupation. Consequently, the % is still not very high, and yet a significant spin exchange, leading to a single EPR signal is observed. This indicates that the distribution of the S_3^- is not homogeneous and suggests that some cooperative interactions may be present.

To summarize, the two different S_3^- signals are a consequence of the uneven distribution of the same S_3^- radical within the sodalite structure. The anisotropic one comes from isolated S_3^-, namely, radicals that do not have S_3^- nearby and therefore do not experience a strong spin exchange interaction, while the isotropic signal is due to S_3^- in regions where several neighboring cages are occupied. As the calcination temperature increases, more SO_4^{2-} anions are reduced and migration of sulfur species becomes easier and the amount of neighboring S_3^- increases. This must be associated with a mechanism which attracts the sulfur anions to close cages at high calcination

temperatures. Finally, the presence of S_2^- could be detected by the FS-ED EPR measurements and the HYSCORE results imply that it interacts only with weakly coupled ^{27}Al or ^{23}Na. This is consistent with its smaller size which allows larger distances from the zeolite framework and the Na^+ cations, located in the center of the six rings.

The ENDOR results show that the isolated S_3^- radicals experience different interactions with ^{23}Na cations. In both BS-I and BS-III a relatively small amount of type (c), weakly coupled, ^{23}Na cations ($\sim$1 MHz) is observed and assigned to rather distant nuclei. In addition, both samples consist of type (b) ^{23}Na nuclei with a coupling of $\langle A_{iso1}\rangle = 2.6 \pm 0.2$ MHz. Finally, BS-I, which has a lower Al/Si value, 0.64, reveals also type (a) ^{23}Na nuclei with strong coupling, $\langle A_{iso2}\rangle = 8 \pm 1$ MHz. We attribute the difference in the ^{23}Na nuclei to isolated S_3^- radicals located in β cages with a different number of Na^+ cations. In BS-III, with the high Al/Si ratio (0.91) and the largest content of Na_{ex}^+, the majority of the cages consist of four Na^+ cations and therefore the S_3^- radicals are in a "symmetric" environment surrounded by four similar Na^+ ions, as represented by the model shown in Figure 9 and suggested earlier by Gobeltz-Hautecoeur et al.[18] These are assigned to the type (b) ^{23}Na nuclei. In contrast, the lower Na_{ex}^+ and Al/Si ratio of BS-I suggests that for a significant number of S_3^- radicals there are less than four ^{23}Na cations in the β cage; therefore the environment becomes less symmetric. This, in turn, leads to a displacement of the radical from the center of the cage and to a higher proximity to the sodium cations, required to stabilize the sulfur anionic charge. Therefore, the corresponding hyperfine coupling is significantly larger, $\langle A_{iso2}\rangle = 8 \pm 1$ MHz. Alternatively, it is possible that in cages with a smaller amount of Na^+ ions and less symmetric arrangements, the $Na-S_3^-$ distances are different, resulting in two types of ^{23}Na nuclei, type (a) and type (b). In this case, however, it is not expected that the ^{23}Na nuclei with the longer distance will give the same coupling as in the symmetric case (2.6 MHz). Therefore we prefer the previous option. In principle, these two options could be distinguished through a correlation experiment, such as the 2D TRIPLE, which provides correlations between nuclei that belong to the same species.[63-67] A similar situation was found by Pierloot and co-workers who have investigated theoretically the location of (extra-framework) Cu-(II) in cluster models representing zeolite six ring sites with different numbers of Al atoms. The models were selected to account for the different *g* factors found in samples with different Al/Si.[63] They found, among others, that in rings containing two Al atoms the Cu(II)-O_1 distances, where O_1 is an oxygen next to Al, are smaller compared to the Cu(II)-O bond in rings containing three framework Al.

For comparison, CW EPR measurements on S_2^- in single crystals of NaCl[68] detected two types of ^{23}Na nuclei, one with $A_{xx} = 4.48$ MHz, $A_{yy} = 3.91$ MHz, and $A_{zz} = 3.34$ MHz and the other with $A_{xx} = -5.35$ MHz, $A_{yy} = -4.05$ MHz, and $A_{zz} = -3.82$ MHz. Similar measurements carried out on NaBr and NaI crystals gave somewhat smaller couplings.[69] In this respect, the significantly larger coupling of 8.1 MHz observed in BS-I is rather remarkable. In this single crystal study the ^{23}Na quadrupole coupling tensor was determined as well. It was found to be significantly different for the two types. While for the first one the magnitude of the largest component was 0.55 MHz, it was close to zero for the second. Unfortunately, in our ENDOR/HYSCORE spectra we could not obtain any information on the quadrupole interaction due to the low resolution.

Formation Mechanism. While most earlier studies focused on the preparation of sodalite with Al/Si = 1, this study shows that various pigments can also be formed with Al/Si < 1. This is possible due to the use of TMAOH as template; otherwise the product of the reaction is usually cancrinite and not sodalite.[66] The template, which is located in part of the β cages, expands the unit cell and possibly facilitates SO_4^{2-} occlusion in the β cage. Moreover, the decomposition of the template during calcination provides reducing agents such as H_2, CO, and hydrocarbons,[64] all used for the reduction of the sulfate anions under high-temperature conditions. Thermal treatment was also shown to produce sulfur-based radicals in the channels of cancrinite prepared with thiosulfate anions. In this case, the reduction occurs via the disproportionation of two adjacent $S_2O_3^{2-}$ anions located in the larger channels of cancrinite.[48]

The relative intensities of the S_3^- and S_2^- signals in the UV–vis spectra are strongly dependent on the calcination conditions and on the Al/Si ratio. This was shown by the preparation of three additional samples, varying either in their synthesis gel composition or in the calcination conditions (see Supplementary Information). In all cases the total radical amount ($S_3^- + S_2^-$), and particularly the amount of S_3^-, was higher for samples calcined at higher temperatures. In two of these samples, calcination for 1 h at 1273 K generated the S_3^- with the isotropic signal; however, it was difficult to reproduce the conditions under which no S_2^- is present (as in BS-I). Ultramarine blue samples that are considered as "pure" and of high quality were found to have an exchange narrowed Lorentzian line,[9] namely, the S_3^- cage occupancy reaches a maximum with no S_2^-. In such commercial samples the S_3^- occupancy, as calculated from quantitative EPR measurements, was found to be less than 50%.[18] Hence, the best preparation conditions required for such a quality of sample using our method of synthesis are yet to be found. The issue of controlling the amount of the various sulfur species needs further detailed experiments in which parameters such as the Al/Si ratio and the relative amounts of TMAOH, Na^+, and SO_4^{2-} will be systematically varied, together with the calcination conditions, and correlated with TGA analyses. It would also be interesting to expand the unique synthesis procedure presented in this work to other color centers such as Se_2^- and Te_2^-.[1] However, preliminary experiments with Na_2SeO_4 and sodium aluminate as the sole Al source, using the formulation for samples I and II, resulted in cancrinite products.

(63) Delabie, A.; Pierloot, K.; Groothaert, M. H.; Schoonheydt, R. A reinterpretation of the ESR spectra of Cu(II) in zeolites A, Y, and ZK4. *Phys. Chem. Chem. Phys.* **2001**, *11*, 2174−2183.
(64) Wu, E. L.; Whyte, T. E., Jr.; Venuto, P. B. Synthetic offretite. II. Decomposition of organic cations and generation of acidity *J. Catal.* **1971**, *21*, 384−393.
(65) Szabo, A.; Ostlund, N. S. *Modern Quantum Chemistry. Introduction to advanced electronic structure theory*; Dover: Mineola, NY, 1989.
(66) Barrer, R. M.; Cole, J. F. Self-entrainment by sodalite and cancrinite during their synthesis. *J. Chem. Soc. A* **1971**, 1516−1523.
(67) Epel, B.; Goldfarb, D. Two-dimensional pulsed TRIPLE at 95 GHz. *J. Magn. Reson.* **2000**, *146*, 196−203.

(68) Van-Doorslaer, S.; Maes; F.; Callens, F.; Matthys; Boesman, E. ENDOR investigation of S_2^-, SSe^- and Se_2^- defects in NaCl. *J. Chem. Soc., Faraday Trans.* **1996**, *92*, 1579−1586.
(69) Van-Doorslaer, S.; Callens, F.; Maes; F.; Boesman, E. Electron−nuclear double-resonance analysis of diatomic sulfur and selenium defects in NaBr and NaI. *Phys. Rev. B* **1996**, *54*, 1145−1152.

Conclusions

A new synthesis of blue ultramarine pigments was reported and S_2^- and three types of S_3^- radicals were identified; their relative amounts depend on the preparation conditions. All S_3^- radicals were characterized by a broad absorption band at 600 nm but exhibited different EPR and/or ENDOR spectra. In two of the samples, calcined below 1100 K, species with the same *rhombic g*-tensor were detected; however W-band ENDOR spectra showed that the number and location of ^{23}Na cations around these species are different. A third radical, characterized by an *isotropic g* was found in a sample calcined at 1273 K. On the basis of DFT calculations of *g*-tensors we assigned all S_3^- radicals observed in this study to S_3^- in an open (C_{2v}) structure, but located at different environments within the sodalite cages. One of the species, found in a sample with Al/Si = 0.91, is well isolated from neighboring radicals and is located inside the zeolite β cage, surrounded by four sodium cations in a distance of about 2.7 Å. An additional species with a similar *g*-tensor found in a sample with Al/Si = 0.64 has 1−3 sodium ligands in a closer proximity. The S_3^- with the isotropic *g* signal was attributed to a "cluster" of S_3^- radicals where several neighboring β cages are occupied, thereby experiencing a substantial exchange interaction. Further exploration of the many variables in this system may well result in new low-toxicity pigments.

Supporting Information Available: Details of the preparation and UV−vis spectra of additional blue ultramarine pigments and the choice of functional and basis set, tables of the ICP elemental analysis and *g*-tensor predictions, and a figure of the UV−vis spectra. This material is available free of charge via the Internet at http://pubs.acs.org.

JA0320121